Journal of Materials Chemistry A

ROYAL SOCIETY OF CHEMISTRY

PAPER

View Article Online
View Journal | View Issue



Cite this: J. Mater. Chem. A, 2022, 10, 19690

# Solvent effect on the Seebeck coefficient of $Fe^{2+}$/$Fe^{3+}$ hydrogel thermogalvanic cells†

Yang Liu, ‡[a] Qi Zhang,‡[a] George Omololu Odunmbaku,‡[a] Yongjie He,[a] Yujie Zheng,[b] Shanshan Chen,[b] Yongli Zhou,[a] Jing Li,[a] Meng Li[a] and Kuan Sun *[a]

Thermogalvanic (TG) cells offer a clean and scalable energy conversion pathway for the recovery of low-grade waste heat. Enhancing the voltage generated by a single TG cell is crucial for widespread application in the internet of things (IoT) and wearable electronics. But the mechanism for manipulating the thermo-voltage is still unclear. In this work, we investigate the solvent effect on the TG performance by introducing nine organic solvents with different Gutmann donor numbers (DNs) into an aqueous $Fe^{2+}$/$Fe^{3+}$ electrolyte. A strong reverse correlation between the solvent DN and the Seebeck coefficient of the TG cell is observed. Among these, the tetramethylene sulfone–$Fe^{2+}$/$Fe^{3+}$ hydrogel TG cell exhibits a Seebeck value of 2.49 mV $K^{-1}$, which is the largest reported value for $Fe^{2+}$/$Fe^{3+}$ based TG cells to date. A combination of experiments and molecular dynamics is used to elucidate the role of solvent DN on the Seebeck values. It is found that the difference in entropy contributions from changing solvation shell sizes as a result of organic solvent addition is the origin of the observed dependency between the Seebeck coefficient and solvent DN. This work provides a new perspective for the enhancement of TG performance, and this approach can be extended to other electrolyte systems and realize the application of TG cells.

Received 8th December 2021
Accepted 4th April 2022

DOI: 10.1039/d1ta10508f

rsc.li/materials-a



## Introduction

Efficient utilization of ubiquitous and abundant low-grade waste heat is crucial for ensuring sustainable development.[1] As a result of the intrinsically low heat-to-work conversion yield attainable from low-temperature waste heat, possible conversion technologies must be efficient and scalable. Thermoelectric technologies utilizing the thermoelectric effect, whereby thermal energy is converted to electrical energy *via* coupled heat and charge transport, are the most promising route for low-grade heat recovery.[2–4] However, most inorganic solid-state TEs work efficiently at high temperatures, and thus are an impractical choice for harvesting low-grade waste heat.[5] In addition, the use of costly rare-earth elements does not satisfy the needed scalability and cost-efficient requirements for harvesting low-grade waste heat.[6,7]

In contrast, liquid-state thermogalvanic (TG) cells are gaining increasing attention due to their flexibility, scalability and cost-effectiveness.[8,9] TG cell operation is based on the thermogalvanic effect in which, under a temperature gradient, the temperature dependent nature of electrochemical redox potentials is utilized to provide steady electrical power.[10,11] Typical TG cells have been shown to generate voltage differences of about 1 mV $K^{-1}$, an order of magnitude greater than conventional solid-state alternatives.[12,13] Thus, series connected TG cells can generate significant voltage output under minute

[a]MOE Key Laboratory of Low-grade Energy Utilization Technologies and Systems, School of Energy & Power Engineering, Chongqing University, Chongqing 400044, China. E-mail: kuan.sun@cqu.edu.cn

[b]State Key Laboratory of Power Transmission Equipment & System Security & New Technology, School of Energy & Power Engineering, Chongqing University, Chongqing 400044, China

† Electronic supplementary information (ESI) available. See https://doi.org/10.1039/d1ta10508f

‡ Y. Liu, Q. Zhang, and G. Odunmbaku contributed equally to this work.

*Prof. Kuan SUN is from 30°19′12″N/105°84′01″E, graduated from the reverse of his surname (NUS), and trained at each letter of his given name (KIT, UniMelb And NUS). He is leading a team namely "Laboratory of Flexible Renewable Energy Materials & Devices" (La FREMDs) at Chongqing University, trying to touch the limit of energy conversion efficiency of flexible photovoltaic cells and soft thermoelectric generators. To learn more about us, please visit our group website: https://www.x-mol.com/groups/LaFREMD.*

temperature differences.[14] The Seebeck coefficient ($S_e$, also known as thermopower), a characteristic parameter gauging the effectiveness of a TG cell, is related to the entropy difference for a redox couple by:[15,16]

$$S_e = \frac{V_{OC}}{\Delta T} = \frac{\Delta S}{nF} \quad (1)$$

where $V_{OC}$ is the open circuit voltage, $\Delta T$ is the temperature difference, $n$ is the number of electrons transferred in the redox reaction, $F$ is Faraday's constant, and $\Delta S$ is the partial molar entropy difference of the redox couple.[17–19] This clearly shows that the thermogalvanic effect is an entropically driven process. It has been reported that the magnitude of $\Delta S$ for transition metal redox couples is dependent on a variety of factors including metal–ligand reorganization, solvent shell reorganization, and spin transition during the redox reaction.[16,20,21]

The performance of a TG cell is determined by three factors, the Seebeck coefficient, electrical conductivity, and thermal conductivity.[8] Among them, the $S_e$ depends on the redox couple in the electrolyte, so there is a lot of work focused on electrolyte additives. For example, Yu *et al.*[22] found that guanidinium induced a thermosensitive crystallization/dissolution of $[Fe(CN)_6]^{4-}$ that provided a persistent concentration gradient for improved $S_e$ and suppressed thermal conductivity, and so achieved the highest Carnot relative efficiency of about 11.1%. Zhou *et al.*[23] used temperature-dependent host–guest interaction to provide a concentration gradient of iodine/triiodide ($I^-$/$I_3^-$) between two electrodes, leading to the eminent improvement of $S_e$ from 0.86 mV $K^{-1}$ to 1.97 mV $K^{-1}$. Duan *et al.*[24] claimed that guanidinium and urea caused solvation shell arrangement of both potassium ferri/ferrocyanide ($[Fe(CN)_6]^{4-}$/$[Fe(CN)_6]^{3-}$) and yielded a significant increase in $S_e$ from 1.4 mV $K^{-1}$ up to 4.2 mV $K^{-1}$. Kim *et al.*[21] added organic solvent with an appropriate solubility parameter to aqueous $[Fe(CN)_6]^{4-}$/$[Fe(CN)_6]^{3-}$ and reported that $S_e$ can be more than doubled to 2.9 mV $K^{-1}$ by significant rearrangement of the solvation shell. Inoue *et al.*[25] systematically investigated the organic solvent influence of aqueous $[Fe(CN)_6]^{4-}$/$[Fe(CN)_6]^{3-}$ and proposed an empirical volume effect, indicating that the solvent effect on $S_e$ is significant.

However, the influence of solvents on redox couple ions is still unclear, and there is no specific and regular mechanism discovered. Furthermore, the study of aqueous $Fe^{2+}$/$Fe^{3+}$ redox-couple systems is relatively new, and $Fe^{2+}$/$Fe^{3+}$ ions without ligands are more suitable for studying the influence of solvent effects on ion partial molar entropy. Theoretical calculations of the aqueous electrolyte system in the absence of additives yielded a predicted $S_e$ value of 1.175 mV $K^{-1}$.[26] Most studies to improve the $S_e$ of $Fe^{2+}$/$Fe^{3+}$ systems concentrate on the influence of the coordinating anions,[27] the addition of structure making/breaking ions,[28] or the influence of pH.[29] Unfortunately, these studies have only generated a modest improvement in the $S_e$, and there is no report that considers the solvent effect from the perspective of organic solvent additives in aqueous $Fe^{2+}$/$Fe^{3+}$ redox-couple TG cells.

According to the Lewis acid–base theory,[30] $Fe^{2+}$/$Fe^{3+}$ as a transition metal cation is an electron acceptor. The Gutmann donor number (DN) is a measure of the strength of solvents as Lewis bases. In general, the tendency of solvent molecules to donate electron pairs can be described by the Gutmann DN.[31,32] Solvent DN has recently proven to be a good descriptor of the electron transfer rates in nucleophilic aromatic substitution reactions to account for the solvent effect.[33] Thus, since $\Delta S$ is related to the reorganization energy of the solvent around the redox ions, it is expected that solvents with varying DNs can modify the solvation shell compared to that in a purely aqueous environment, and lead to changes in $\Delta S$ for the redox couple.

Herein, we introduce organic solvents with different DNs into 0.01 M $Fe^{2+}$/$Fe^{3+}$ electrolyte in polyacrylamide (PAAm) hydrogel. An inverse relationship between $S_e$ of the aqueous $Fe^{2+}$/$Fe^{3+}$ electrolyte and DN is observed. Specifically, $S_e$ drops to 0.74 mV $K^{-1}$ upon the addition of a high DN solvent, and conversely, the addition of a low DN solvent yields a dramatically increased $S_e$ value of 2.49 mV $K^{-1}$. Experiments combined with molecular dynamics simulation suggest that entropy contributions from changing solvation shell sizes as a result of organic solvent addition are the origin of the observed dependency between $S_e$ and solvent DN. This work elucidates the crucial importance of solvent DN and opens up new avenues for the improvement of the Seebeck coefficient of $Fe^{2+}$/$Fe^{3+}$ based TG cells.

## Results and discussion

### Seebeck coefficient of the TG cell

The working process of the $Fe^{2+}$/$Fe^{3+}$ TG cell is shown in Fig. 1a. The TG cell originates from the entropy difference of redox couples. Taking the $Fe^{2+}$/$Fe^{3+}$ redox couple as an example, $Fe^{3+}$ has a higher charge density, resulting in a more compact hydration shell with lower thermodynamic entropy than $Fe^{2+}$. Therefore, when a temperature gradient is applied at both sides of the electrodes, the oxidation of $Fe^{2+}$ to $Fe^{3+}$ releases electrons to the electrode at the cold side, and the electrons pass through the external circuit to the hot side, where reduction of $Fe^{3+}$ to $Fe^{2+}$ occurs. Due to the ion concentration difference established between the two electrodes, each redox species will diffuse towards the respective electrode, so the TG cell can work continuously to generate voltage.

In order to investigate the influence of organic solvents on the TG cell performance, nine solvents with varying DNs were chosen for this work: tetramethylene sulfone (TLS), acetone (CP), methanol (MeOH), ethylene glycol (EG), isopropyl alcohol (IPA), *N*,*N*-dimethylformamide (DMF), *N*-methylpyrrolidone (NMP), dimethyl sulfoxide (DMSO), and *N*,*N*-diethylformamide (DEF). The organic solvents were mixed with 0.01 M $Fe^{2+}$/$Fe^{3+}$ aqueous electrolyte at 6 mol% individually, and the resulting electrolyte solution was incorporated into PAAm polymer to form a microporous hydrogel that avoids leakage issues and facilitates TG cell assembly. Further experimental details can be found in the Experimental section. The physical parameters of the selected solvents, such as melting point, dielectric constant, *etc.*, are listed in Table S1.† A schematic diagram of the specific sample preparation process is also shown in the Experimental section.

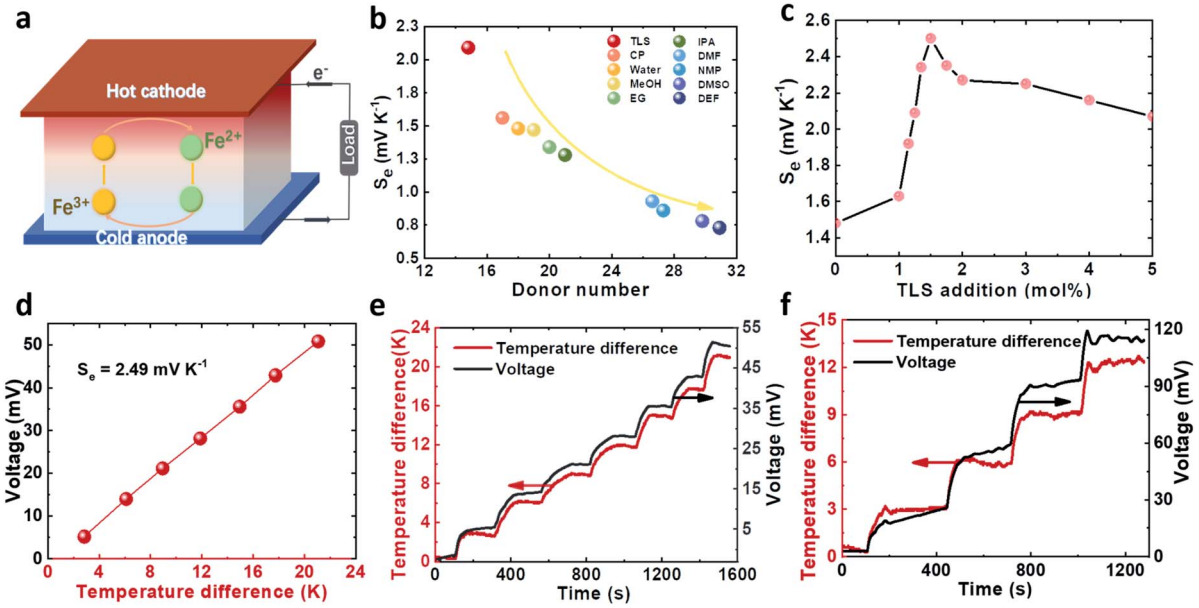


Fig. 1 (a) Schematic of a hydrogel thermogalvanic cell containing the $Fe^{2+}/Fe^{3+}$ redox couple. (b) $S_e$ of hydrogels with the $Fe^{2+}/Fe^{3+}$ redox couple in organic–water solutions with 6 mol% organic solvent additives with different DNs. (c) Dependence of the $S_e$ on TLS concentration. (d) Change of the open circuit voltage for hydrogels with 1.5 mol% TLS and $Fe^{2+}/Fe^{3+}$ electrolyte with changing temperature difference from 0 to 20 K. (e) Time evolution of the thermo-voltage of the hydrogel with 1.5 mol% TLS and $Fe^{2+}/Fe^{3+}$ electrolyte under a sequence of temperature differences. (f) Voltage output of a thermoelectric device under different temperature gradients.

From Fig. 1b and Table 1, the $S_e$ of the pristine 0.01 M $Fe^{2+}/Fe^{3+}$ gel-based TG cell is 1.48 mV $K^{-1}$, which is in agreement with the previous report in purely aqueous liquid-electrolyte based TG cells.[29] This implies that there is a negligible difference between $S_e$ values obtained from gel-based and liquid-electrolyte based TG cells. It is clear from Fig. 1b that there exists a monotonic decrease in the $S_e$ value of the TG cell with increasing DN of the organic solvent additive. From Table 1, DEF with the largest DN of 30.9 exhibits an $S_e$ value as low as 0.73 mV $K^{-1}$. Upon switching to organic solvent additives with decreasing DN, the $S_e$ value rises to 2.09 mV $K^{-1}$ for TLS, which has a DN of 14.8.

Since the TLS additive exhibited the best performance, it is imperative to determine the optimal TLS content. The dependence of the electrochemical thermopower of the 0.01 M $Fe^{2+}/Fe^{3+}$ TG cell on different TLS contents is shown in Fig. 1c. The $S_e$ value sharply rises to a maximum value of 2.49 mV $K^{-1}$ upon the addition of 1.5 mol% TLS followed by a slow decrease on further addition of TLS. The electrochemical thermopower still remained above 2 mV $K^{-1}$ at a TLS content of 6 mol%. It is worth noting that the optimal $S_e$ value of 2.49 mV $K^{-1}$ is the highest Seebeck coefficient among all $Fe^{2+}/Fe^{3+}$ thermogalvanic cells reported to date.

Based on the optimized 1.5 mol% TLS $Fe^{2+}/Fe^{3+}$ hydrogel, Fig. 1e demonstrates the thermal voltage variation of a single TG cell with a temperature difference, which indicates that the voltage signal of the TG cell responds rapidly to temperature change, and the $S_e$ value is 2.49 mV $K^{-1}$ at 1.5 mol% TLS addition. Meanwhile, we made a thermoelectric device by Z-type connection of four single TG cells with a carbon cloth electrode. Fig. 1f shows the device performance under different temperature gradients. The voltage signal is still sensitive to temperature variations. Furthermore, there is no prominent voltage loss after the connection in series, *e.g.* the $S_e$ value of devices with 4 TG cells is about $9.99 \pm 0.46$ mV $K^{-1}$, which is almost quadruple the $S_e$ of a single cell (2.49 mV $K^{-1}$). This clearly demonstrates the viability of TLS organic solvent additives for boosting the thermogalvanic performance of $Fe^{2+}/Fe^{3+}$ electrolytes and opens up promising avenues for IoT and wearable technology applications.

Table 1 Seebeck coefficient of the 0.01 M $Fe^{2+}/Fe^{3+}$ redox couple in organic–water solutions (standard deviation was obtained from three measured samples). The organic solvent content is 6 mol% with respect to total water content

| Solvent | Donor number[32,34] | Seebeck coefficient (mV $K^{-1}$) |
|---|---|---|
| Tetramethylene sulfone | 14.8 | $2.09 \pm 0.03$ |
| Acetone | 17 | $1.57 \pm 0.01$ |
| $H_2O$ | 18 | $1.48 \pm 0.01$ |
| Methanol | 19 | $1.47 \pm 0.01$ |
| Ethylene glycol | 20 | $1.34 \pm 0.05$ |
| Isopropyl alcohol | 21 | $1.28 \pm 0.06$ |
| *N*,*N*-Dimethylformamide | 26.6 | $0.93 \pm 0.06$ |
| *N*-Methylpyrrolidone | 27.3 | $0.86 \pm 0.05$ |
| Dimethyl sulfoxide | 29.8 | $0.78 \pm 0.03$ |
| *N*,*N*-Diethylformamide | 30.9 | $0.73 \pm 0.06$ |

## Electrochemical properties of the $Fe^{2+}/Fe^{3+}$ redox couple

In order to obtain an insight into the redox reactions taking place at the electrodes, temperature-dependent cyclic

 

voltammetry tests were conducted using an isothermal electrochemical cell with three electrodes. The open circuit potential of thermogalvanic cells is derived from the temperature dependent shift in the equilibrium potential of the redox reaction.[35] Therefore, the $S_e$ of the TG cell is the temperature coefficient of the redox couples, which can be obtained from eqn (2).[36] According to the Nernst equation, the formal potential ($E$) of the redox reaction can be expressed as eqn (3). In addition, the formal potential can be obtained by averaging the potentials of cathodic and anodic peaks in a cyclic voltammetry measurement. Therefore, the slope of the plot of the formal potential as a function of temperature should be roughly consistent with the measured thermopower value.

$$S_e = \frac{dE}{dT} \quad (2)$$

$$E = E^0 + \frac{RT}{nF} \ln \frac{\alpha_{ox}}{\alpha_{red}} \quad (3)$$

where $E^0$ is the standard potential, $\alpha_{ox}$ and $\alpha_{red}$ are the activities of redox couple ions, respectively, and $R$ is the ideal gas constant.

Fig. 2a and b present the cyclic voltammograms of 0.01 M $Fe^{2+}/Fe^{3+}$ electrolyte with 6 mol% TLS and 6 mol% DMSO, respectively, from 20 °C to 60 °C. It is obvious from these figures that the oxidation and reduction peak-to-peak separation decreases with increasing temperature. Furthermore, the temperature dependent shift in the reduction potential is the dominant contributing factor for the shift in the equilibrium potential and in turn, the observed changes in $S_e$ values. This is consistent with the reduction reaction that occurs at the hot side of the $Fe^{2+}/Fe^{3+}$ thermal cell, which can also be reflected by the positive sign of $S_e$.

In the absence of organic solvent additives, the oxidation potential similarly shows a very weak dependence on temperature, with a gradual enhancement of the reduction potential in the pristine sample (Fig. S2†). The slope of the intermediate potential line fit from Fig. S2† is 1.7 mV $K^{-1}$, and subtracting the temperature coefficient of the Ag/AgCl reference electrode (0.2 mV $K^{-1}$) from this term yields a thermopower of 1.5 mV $K^{-1}$ for 0.01 M $Fe^{2+}/Fe^{3+}$, which is consistent with the results from the pristine TG cell in Table 1. In the presence of 6 mol% TLS, the reduction potential exhibits a steep increase especially at high temperatures with minimal variation in oxidation potential (Fig. 2c). Here, the slope of the $E_{1/2}$ potential is 2.29 mV $K^{-1}$, and considering the temperature coefficient of the Ag/AgCl reference electrode, this result (2.09 mV $K^{-1}$) also agrees well with the measured $S_e$ value of the 6 mol% TG cell at 2.09 mV $K^{-1}$ from Table 1. In the case of 6 mol% DMSO, the gentle increase in the reduction potential is accompanied by a slight but non-negligible decrease in the oxidation potential (Fig. 2d). Excluding the temperature coefficient of the reference electrode, the Seebeck value is only 0.8 mV $K^{-1}$.

From the temperature-dependent cyclic voltammetry tests, the $S_e$ value can be confirmed and the dependence of equilibrium potential with temperature can be easily concluded. It further proves that the $S_e$ of TG cells is dominated by redox reactions.

### Characterization of the Fe ion solvent shell

In aqueous solutions containing non-coordinating anions such as perchlorates, both ferrous and ferric ions possess a primary

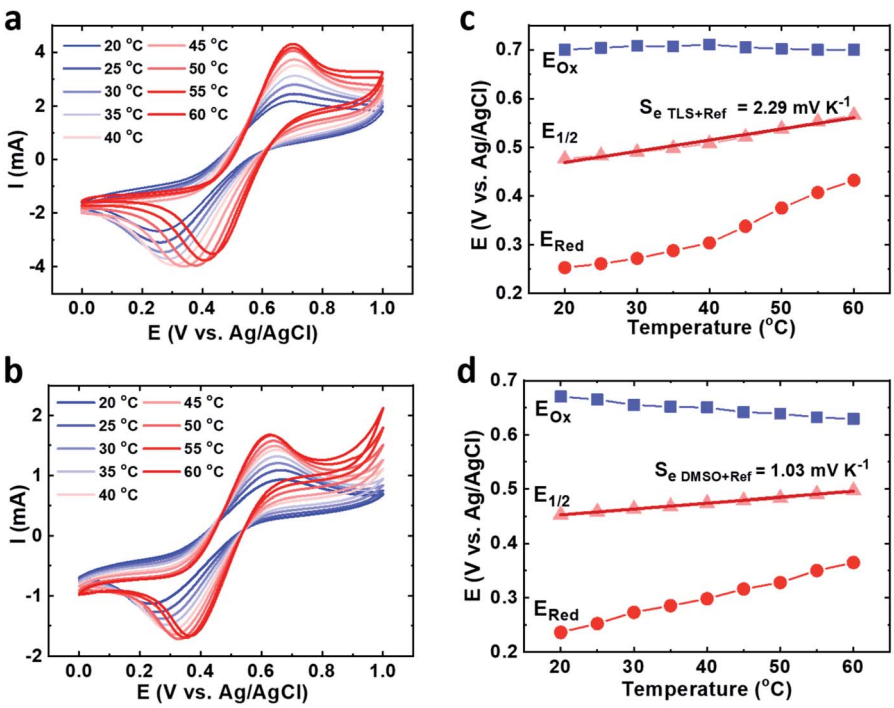


Fig. 2 Cyclic voltammograms of 0.01 M $Fe^{2+}/Fe^{3+}$ with (a) 6 mol% TLS addition and (b) 6 mol% DMSO addition. The plot of $E_{1/2}$ and peak potential of reduction reactions at various temperatures at (c) 6 mol% TLS addition and (d) 6 mol% DMSO addition.

solvation shell consisting of six water molecules, and there is a hydrolysis reaction of metal ions,[37] where the hydrolysis of the $Fe^{3+}$ complexes would result in a deprotonated $Fe(H_2O)_5(OH)^{2+}$, as illustrated below:

$$Fe(H_2O)_6^{3+} \rightarrow Fe(H_2O)_5(OH)^{2+} + H^+$$

Because of this hydrolysis reaction, the transformation of the ionic solvent shell should cause a change in pH value, as well as a change in the valence state of the ion that might be reflected in the light absorption profile.

The pH of solutions containing 0.1 M $Fe(ClO_4)_3$, in the absence or presence of 20 vol% of organic solvent, was measured and the results are summarized in Fig. 3a. A correlation between the DN and pH clearly exists, with the pH value of the solution decreasing with lower DN values. More specifically, the addition of organic solvents with DN lower than that of water results in a lower solution pH and is indicative of stronger $Fe(H_2O)_6^{3+}$ hydrolysis. On the other hand, solvents with larger DN interact more strongly with $Fe^{3+}$ ions compared to water, thereby reducing the hydrolysis effect and increasing the pH. It is interesting to note that IPA does not seem to conform to this trend. This is because it is a protic solvent, and can therefore be hydrolyzed when combined with iron ions. Fig. 3b shows a monotonic decrease in pH with increasing content of TLS in the 0.1 M $Fe^{3+}$ aqueous solution, which confirms that an organic solvent with a small DN can facilitate the hydrolysis of the $Fe^{3+}$ complexes.

In order to further observe the transformation of the solvent shell, UV-vis spectra of 1 mM $Fe^{3+}$ solution with varying TLS content were obtained (Fig. 3c). The peak at ~200 nm belongs to TLS, and the absorption peak at 290 nm is attributed to $Fe(H_2O)_5(OH)^{2+}$.[37] As the TLS content increased, the intensity of the 290 nm peak became stronger, showing that $Fe^{3+}(H_2O)_6$ hydrolysis is gradually enhanced. This observation is in agreement with the pH measurement results (Fig. 3b). Furthermore, two small peaks near 458 nm and 570 nm appear upon the addition of TLS corresponding to a sulfolane molecule containing two oxygen atoms and this could possibly be ascribed to TLS–$Fe^{3+}$ complexes.

In the case of high DN DMSO solvent addition, the pH of the 0.1 M $Fe^{3+}$ solution gradually rises as expected (Fig. 3d), with a steeper rate than the case of TLS addition. DMSO shows a very strong and broad absorption band starting at 250 nm (Fig. 3e), so it overlaps with the peak features of $Fe(H_2O)_6^{3+}$ at around 200 nm.[37] Nevertheless, it is obvious that after adding DMSO, due to the strong coordination effect of DMSO and $Fe^{3+}$, a new absorption peak appears at 265 nm, and the peak intensity is much higher than those of the characteristic peaks of $Fe(H_2O)_6^{3+}$ or $Fe(H_2O)_5(OH)^{2+}$. With the increase of DMSO addition, the strength of this peak continues to increase, consistent with the pH measurements. The results show that Fe ions are more inclined to interact with DMSO solvent molecules than with water, thereby leading to reduced hydrolysis of $Fe^{3+}$ ions.

### Molecular dynamics simulation of the iron ion

$S_e$ is determined by the entropy difference $\Delta S$ of the redox couple and, in turn, the entropy difference is related to the nature of the ion and the interaction between the ion and the

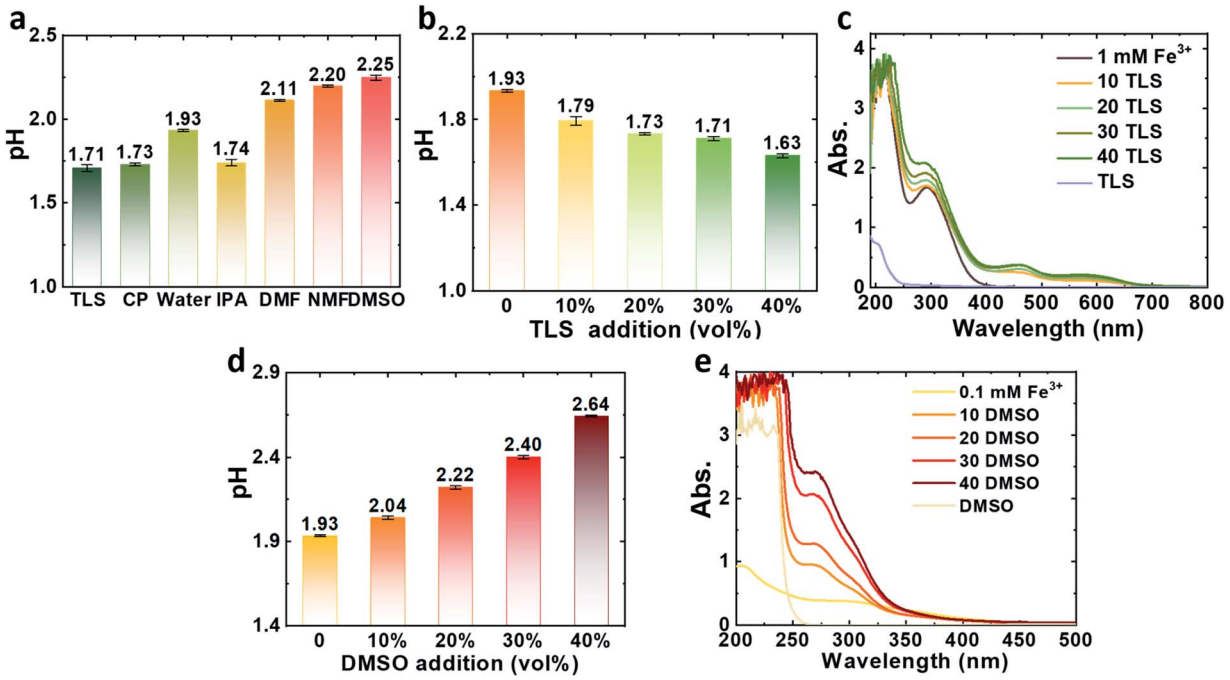


Fig. 3 (a) The pH of the 0.1 M $Fe^{3+}$ electrolyte with 20 vol% of various organic solvents. (b) The pH of the 0.1 M $Fe^{3+}$ electrolyte as a function of TLS content. (c) UV-vis spectra of 1 mM $Fe^{3+}$ electrolyte with varying TLS content. (d) The pH of 0.1 M $Fe^{3+}$ electrolyte as a function of DMSO content. (e) UV-vis spectra of 0.1 mM $Fe^{3+}$ electrolyte with varying DMSO content.

 

solvent molecules. According to Powell,[19] the molar entropy of an ion in an aqueous environment is related to ion charges and the effective ionic radius. Furthermore, ions exist in the form of solvated ions in a solution rather than as bare ions, so the radius should include the coordinated solvent molecules, especially for transition metal cations.[16] To clarify the underlying evolution of the solvent shell, we employed molecular dynamics to simulate the dissolution environment of Fe ions in the presence and absence of organic solvents. For cations, the ion–oxygen atom distance can be used to characterize the ion hydration shell, and the radius of the first solvation shell ($R_1$) can be defined as the distance from the ion to the first minimum in the ion–oxygen atom distribution functions.[38] Thus, the ion–oxygen atom radial distribution function ($g(r)$, probability of finding the oxygen atom at each radius[39]) and coordination number of O atoms around the Fe ion were calculated to monitor changes in the solvent shell as organic solvent molecules were added. The details of the simulation are described in the Experimental section. In the simulation, one organic solvent molecule was inserted into the first solvent shell to replace one water molecule, shown in Fig. 4a and d. From the $g(r)$ (Fig. S3a–c†), it is clear that the solvation structure is mostly limited to the first solvent shell, which corresponds to the first and the strongest peak.

The first peak of $g(r)$ between the $Fe^{2+}/Fe^{3+}$ and O atoms in the TLS–water system, DMSO–water system and water-only system is shown in Fig. 4b and e and S3d.† The higher valence state of $Fe^{3+}$ results in a more tightly packed solvation shell, so the $R_1$ of $Fe^{3+}$ is approximately 2.17 Å and the $R_1$ of $Fe^{2+}$ is roughly 2.37 Å. The radius difference in the first hydration shells of $Fe^{2+}/Fe^{3+}$ in pure water is about 0.2 Å, which is in good agreement with a previous report.[40] As a result of its low donor number, TLS has a weak interaction with $Fe^{3+}$ compared to water upon addition to the solution. Thus, the other five water molecules are more tightly bound by $Fe^{3+}$ and the coordination interaction between $Fe^{3+}$ and water molecules is stronger, leading to a reduced pH value and enhanced hydrolysis in the TLS–water system. This phenomenon is clearly illustrated in Fig. 4b, wherein the first peak separation between the $Fe^{2+}$ and $Fe^{3+}$ ions' $g(r)$ is greater, compared to that of the DMSO–water system. This is primarily a result of the downshift in the first peak valley position of $Fe^{3+}$ to 2.13 Å leading to $Fe^{3+}$ ions having a more closed solvent shell in the TLS–water system. In contrast, the influence of TLS is not as significant in the case of $Fe^{2+}$ due to its smaller charge density relative to $Fe^{3+}$. The $R_1$ of $Fe^{2+}$ only slightly increases to 2.39 Å. Therefore, the radius difference of the first solvent shell of $Fe^{2+}/Fe^{3+}$ increased to 0.26 Å in the TLS–water system. The reverse case appears in the DMSO–water system.

DMSO has a larger DN and therefore interacts more strongly with $Fe^{3+}$ ions, causing the surrounding water molecules to be expelled. This results in the $R_1$ of $Fe^{3+}$ increasing to 0.25 Å in the DMSO–water system (Fig. 4e) and corresponds to a pH increase and decreased hydrolysis. Meanwhile, the $R_1$ of $Fe^{2+}$ (2.39 Å) in

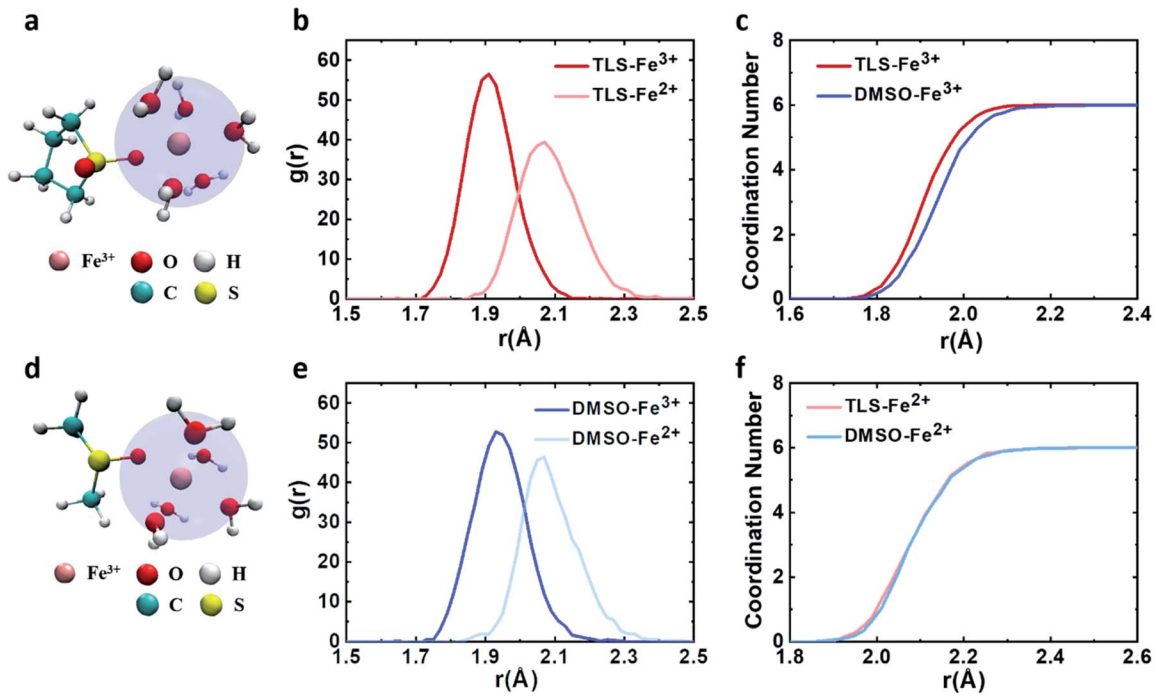


Fig. 4 (a) First solvation shell of the $Fe^{3+}$ with TLS added into the electrolyte. The pink, red, silver, yellow, and green spheres represent Fe, O, H, S, and C atoms, respectively. (b) The first peak of $g(r)$ of the O atoms around Fe ions in the electrolyte with TLS: $Fe^{3+}$ (deep red line) and $Fe^{2+}$ (pink line). (c) The number of coordinating O atoms counted from the $Fe^{3+}$ ion center: with TLS–water solvation (deep red line) and with DMSO–water solvation (deep blue line). (d) First solvation shell of the $Fe^{3+}$ with DMSO added into the electrolyte. (e) The first peak of $g(r)$ of the O atoms around Fe ions in electrolyte with DMSO: $Fe^{3+}$ (deep blue line) and $Fe^{2+}$ (sky blue line). (f) The number of coordinating O atoms counted from the $Fe^{2+}$ ion center: with TLS–water solvation (pink line) and with DMSO–water solvation (sky blue line).

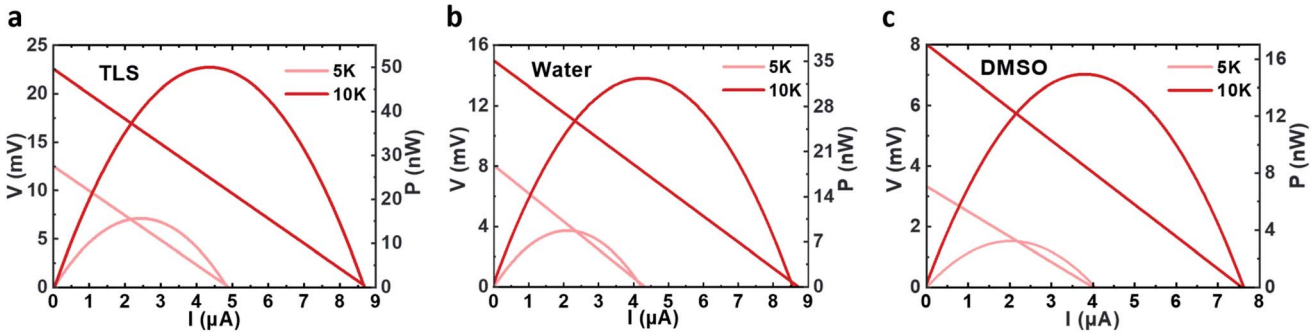


Fig. 5 Voltage output and the corresponding power output for $Fe^{2+}/Fe^{3+}$ TG cells with (a) 6 mol% TLS addition, (b) aqueous solution and (c) 6 mol% DMSO addition under temperature differences of 5 K and 10 K.



the DMSO–water system remains the same as that in the TLS–water system. Thus, the radius difference of the first solvent shell of $Fe^{2+}/Fe^{3+}$ decreased to 0.14 Å. By comparing the Seebeck coefficients in both systems, it can be seen that $S_e$ values increase as the first solvent shell radius difference gradually increases.

The O atom coordination numbers were obtained by integrating the $g(r)$ of the corresponding ion–O RDFs. Comparing the coordination number curves of $Fe^{3+}$ in different solvent environments (Fig. 4c) clearly indicates that the distance between O atoms and $Fe^{3+}$ is shorter in the TLS–water system. This is a result of greater interaction and smaller solvent shell radius. However, the curves of the coordination number of $Fe^{2+}$–O basically coincide (Fig. 4f), indicating that the solvent molecule DN has little effect on the structure of the $Fe^{2+}$ solvent shell. These results are consistent with the conclusion, from the RDF of $Fe^{2+}$–O, that the $R_1$ of $Fe^{2+}$ in the TLS–water and DMSO–water systems are identical.

Based on the experimental and theoretical results, it is clear that the introduction of different DN organic solvent molecules into the aqueous electrolyte system affects the arrangement of water molecules within the inner solvation shell. The change in solvation radius of the Fe ion eventually leads to a change in entropy difference, $\Delta S$, of the redox couple. In the TLS–water system, the radius of the $Fe^{3+}$ ion solvent shell is smaller, which causes the entropy difference in the $Fe^{2+}/Fe^{3+}$ redox couple to increase, leading to a boost in thermopower. In the DMSO–water system, the radius of the $Fe^{3+}$ ion solvent shell increases, so that $\Delta S$ decreases and results in a lower Seebeck value. Therefore, the key underlying mechanism for the enhancement of thermopower *via* organic solvent additives is as follows: the radius of the inner solvation shell is dependent on the electron density donating ability of the surrounding solvating molecules, while the entropy of a redox ion is inversely dependent on the solvation shell size. Thus, low DN solvents interact weakly with Fe ions, thereby allowing water molecules to interact more strongly with the Fe ion and this results in a smaller solvation shell radius. This induces a significant increase in the entropy difference of the redox couple ions. The reverse happens in the case of high DN solvents. This reveals the observed relationship between solvent DN and the measured Seebeck coefficients of the TG cells. To our knowledge, this is the first report elucidating solvent effects in $Fe^{2+}/Fe^{3+}$ based TG cells. This approach offers a rational design route for the enhancement of thermopower.

### The output voltage, current, and power of the hydrogel TG cells

Finally, we demonstrate the applicability of the hydrogel TG cells (Fig. S4†), which can be modified easily into different shapes and is beneficial for integration and packaging without leakage. The output performance of three gels containing different electrolytes is shown in Fig. 5a–c. In the measurement, the cold side temperature was kept constant, and the temperature differences were 5 K and 10 K, respectively. The purely aqueous gel without organic solvent added produced an output voltage of 15 mV under a temperature difference of 10 K, consistent with its $S_e$ value (Fig. 5b). Upon adding 6 mol% TLS to the electrolyte, the output voltage of the gel increased to 22 mV under the same temperature difference of 10 K (Fig. 5a). In the case of the 6 mol% DMSO-based TG cell, the open circuit voltage was only about 8 mV at a temperature difference of 10 K, and the output power also drops accordingly. This clearly shows the importance of solvent interactions on the thermogalvanic properties in $Fe^{2+}/Fe^{3+}$ systems and opens up a new pathway for the rational design of solvation environments for boosting the cell potential of TG cells.

## Conclusions

Our work demonstrates the influence of solvent molecule additives on solvation shell dynamics from the perspective of the Gutmann donor number of solvents. The interplay between solvent DN and solvation shell size, through the entropy dependence on solvent shell radius, creates an inverse relationship between the Seebeck coefficient of the thermogalvanic cell and solvent additive DN. This approach led to an enhancement in the Seebeck coefficient of $Fe^{2+}/Fe^{3+}$ electrolyte hydrogel thermogalvanic cells up to a value of 2.49 mV $K^{-1}$ upon the addition of 1.5 mol% TLS to the aqueous electrolyte. This is the highest reported Seebeck coefficient of $Fe^{2+}/Fe^{3+}$ hydrogel-based thermogalvanic cells. Our solvent DN analysis approach can be extended to enhance the thermogalvanic properties of

 

other electrolyte systems for the efficient conversion of low-grade waste heat into electricity.

# Experimental section

### Materials and measurements

**Materials.** Iron(II) perchlorate hydrate ($Fe(ClO_4)_2 \cdot xH_2O$), iron(III) perchlorate hydrate ($Fe(ClO_4)_3 \cdot xH_2O$), acrylamide (AAM, monomer), crosslinker *N*,*N*′-methylenebis(acrylamide) (*N*,*N*-MBA), α-ketoglutaric acid (KGA, initiator), tetramethylene sulfone (TLS), acetone (CP), methanol (MeOH), ethylene glycol (EG), isopropyl alcohol (IPA), *N*,*N*-dimethylformamide (DMF), *N*-methylpyrrolidone (NMP), dimethyl sulfoxide (DMSO), and *N*,*N*-diethylformamide (DEF) were purchased from Sigma Aldrich and used without further purification. A carbon cloth electrode with an electrical resistivity of less than 13 μΩ $cm^2$ was purchased from Taiwan CeTech Material Company (Taiwan, China). The deionized water used in all experiments was prepared by an ATSro 10.

**Preparation of hydrogel.** A mixed solution was prepared with 2 M acrylamide (AAM) as the monomer, 0.001 M *N*,*N*-MBA as the cross-linking agent, and 0.002 M KGA as the ultraviolet initiator. Then, the solution was deoxygenated with nitrogen for 30 minutes and transferred into a Petri dish for irradiation with 365 nm ultraviolet light for about two hours to obtain the polyacrylamide (PAAm) hydrogel. The formed gel is placed in a 60 °C oven to remove the water inside. Subsequently, the dehydrated hydrogel was soaked in a mixed solution of 0.01 M $Fe(ClO_4)_2/Fe(ClO_4)_3$ and 0.01 M $Fe(ClO_4)_2/Fe(ClO_4)_3$ with various amounts of organic solvent until it was completely swollen.

**Seebeck coefficient measurements.** The Seebeck coefficient was obtained by the potential difference across the electrodes, with a thermal gradient at the upper and lower ends of the gel. In order to ensure adequate conductivity of the electrode, a carbon cloth electrode is used. The open circuit voltage was measured with a Keithley 2700, and the temperature difference data were collected using a thermocouple data logger (USB-TC-08, Pico Technology, St. Neots, UK). In the stepped heating, the voltage under different temperature differences is measured, and the temperature difference and voltage readings were maintained for at least 100 s and averaged to ensure the accuracy of the Seebeck test.

**Electrochemical measurements.** The cyclic voltammetry at different temperatures to measure the formal potential of redox ions was performed using a Bio-Logic VMP3 (SN 0897) three-electrode setup with a platinum tablet electrode as the working electrode, and carbon rod electrode as the auxiliary electrode, and an Ag/AgCl reference electrode. The voltage window range was from 0 V to 1 V, and the scan rate was 10 mV $s^{-1}$. The working and auxiliary electrodes were fully immersed in the cell. The temperature was precisely controlled using a water bath heater, while the reference electrode was placed at an ambient temperature of 20 °C.

**Power output measurement.** Linear sweep voltammetry (LSV) was conducted to measure the current and power output at different temperatures. LSVs were measured using a Bio-Logic VMP3 (SN 0897) two-electrode setup. The scans started from the $V_{OC}$ (as measured by the Bio-Logic VMP3), then scanned to V = 0 V. The standard step size of 0.0025 V was employed, and a scan rate of 0.1 mV $s^{-1}$ investigated.

### Solvent shell characterization and simulation

**Spectroscopy and pH measurements.** UV-vis spectra were obtained using a UV-Vis spectrophotometer (Shimadzu UV-1800) in the 200–800 nm range, utilizing quartz cells with a path length of 10 mm. The pH was measured using a Leici PHS-2F.

**Simulation.** Molecular dynamics simulation was performed using the semiempirical extended tight-binding program package xTB. The GFN2-xTB method was used to simulate the system for 100 ps at 298.15 K. The simulation step is 1 fs and snapshots along the trajectory were obtained every 0.1 ps. To keep the molecules from escaping, the simulation was confined in a little sphere. The system contains 1 Fe ion, 95 water molecules and 5 second solvent molecules or 1 Fe ion and 100 water molecules in the water system. The visualization and analysis of the trajectories was done by VMD. The Radial Distribution Function (RDF) was calculated using the last 100 frames of the molecular dynamics trajectories. We simulated the electrolytes using a computational box (20 × 20 × 20 Å) that is composed of about 350 atoms with periodic boundary conditions in all directions. The coordination number was obtained according to the equation:

$$n_x(R) = 4\pi\rho_x \int_0^R g_x(r) r^2 \mathrm{d}r$$

where $\rho_x$ is the average number density of the species x. And for the first solvent shell, $R$ is the position of the first minimum position of $g(r)$ after the first peak.

# Author contributions

Y. L., Y. H., S. C. and Y. L. Z. carried out the experiments and analysed the data. Q. Z. and Y. J. Z. performed molecular dynamics calculations and analysed computational data. Y. L., G. O. O. and K. S. prepared and revised the manuscript. J. L. and M. L. provided experimental support. K. S. supervised the project. All authors discussed the results and commented on the manuscript.

# Conflicts of interest

There is no conflict to declare.

# Acknowledgements

This work was financially supported by research grants from the National Natural Science Foundation of China (62074022, 12004057, and 52173235), Natural Science Foundation of Chongqing (cstc2021jcyj-jqX0033, cstc2021ycjh-bgzxm0334, and CQYC2021059206), Fundamental Research Funds for the Central Universities (2020CDJQY-A055 and 2020CDJ-LHZZ-044)

and the Key Laboratory of Low-Grade Energy Utilization Technologies and Systems (LLEUTS2019001).

## References

1 C. Forman, I. K. Muritala, R. Pardemann and B. Meyer, *Renewable Sustainable Energy Rev.*, 2016, **57**, 1568–1579.
2 J. P. Heremans, *Nature*, 2014, **508**, 327–328.
3 M. Haras and T. Skotnicki, *Nano Energy*, 2018, **54**, 461–476.
4 J. Mao, H. T. Zhu, Z. W. Ding, Z. H. Liu, G. A. Gamage, G. Chen and Z. F. Ren, *Science*, 2019, **365**, 495–498.
5 X. Shi and J. He, *Science*, 2021, **371**, 343–344.
6 S. K. Yee, S. LeBlanc, K. E. Goodson and C. Dames, *Energy Environ. Sci.*, 2013, **6**, 2561–2571.
7 S. LeBlanc, S. K. Yee, M. L. Scullin, C. Dames and K. E. Goodson, *Renewable Sustainable Energy Rev.*, 2014, **32**, 313–327.
8 J. J. Duan, B. Y. Yu, L. Huang, B. Hu, M. Xu, G. Feng and J. Zhou, *Joule*, 2021, **5**, 768–779.
9 M. F. Dupont, D. R. MacFarlane and J. M. Pringle, *Chem. Commun.*, 2017, **53**, 6288–6302.
10 T. I. Quickenden and C. F. Vernon, *Sol. Energy*, 1986, **36**, 63–72.
11 T. I. Quickenden and Y. Mua, *J. Electrochem. Soc.*, 1995, **142**, 3985–3994.
12 L. R. Liang, H. C. Lv, X. L. Shi, Z. X. Liu, G. M. Chen, Z. G. Chen and G. X. Sun, *Mater. Horiz.*, 2021, **8**, 2750–2760.
13 Z. Lei, W. Gao and P. Wu, *Joule*, 2021, **5**, 2211–2222.
14 P. H. Yang, K. Liu, Q. Chen, X. B. Mo, Y. S. Zhou, S. Li, G. Feng and J. Zhou, *Angew. Chem., Int. Ed.*, 2016, **55**, 12050–12053.
15 E. L. Yee and M. J. Weaver, *Inorg. Chem.*, 1980, **19**, 1077–1079.
16 E. L. Yee, R. J. Cave, K. L. Guyer, P. D. Tyma and M. J. Weaver, *J. Am. Chem. Soc.*, 1979, **101**, 1131–1137.
17 E. D. Eastman, *J. Am. Chem. Soc.*, 1928, **50**, 292–297.
18 N. Sutin, M. J. Weaver and E. L. Yee, *Inorg. Chem.*, 1980, **19**, 1096–1098.
19 R. E. Powell and W. M. Latimer, *J. Chem. Phys.*, 1951, **19**, 1139–1141.
20 T. J. Abraham, D. R. MacFarlane and J. M. Pringle, *Energy Environ. Sci.*, 2013, **6**, 2639–2645.
21 T. Kim, J. S. Lee, G. Lee, H. Yoon, J. Yoon, T. J. Kang and Y. H. Kim, *Nano Energy*, 2017, **31**, 160–167.
22 B. Yu, J. Duan, H. Cong, W. Xie, R. Liu, X. Zhuang, H. Wang, B. Qi, M. Xu, Z. L. Wang and J. Zhou, *Science*, 2020, **370**, 342–346.
23 H. Zhou, T. Yamada and N. Kimizuka, *J. Am. Chem. Soc.*, 2016, **138**, 10502–10507.
24 J. J. Duan, G. Feng, B. Y. Yu, J. Li, M. Chen, P. H. Yang, J. M. Feng, K. Liu and J. Zhou, *Nat. Commun.*, 2018, **9**, 1–8.
25 D. Inoue, Y. Fukuzumi and Y. Moritomo, *Jpn. J. Appl. Phys.*, 2020, **59**, 037001.
26 T. Migita, N. Tachikawa, Y. Katayama and T. Miura, *Electrochemistry*, 2009, **77**, 639–641.
27 K. Kim, S. Hwang and H. Lee, *Electrochim. Acta*, 2020, **335**, 135651.
28 B. T. Huang, S. Muy, S. T. Feng, Y. Katayama, Y. C. Lu, G. Chen and Y. Shao-Horn, *Phys. Chem. Chem. Phys.*, 2018, **20**, 15680–15686.
29 M. A. Buckingham, F. Marken and L. Aldous, *Sustainable Energy Fuels*, 2018, **2**, 2717–2726.
30 R. G. Pearson, *J. Am. Chem. Soc.*, 1963, **85**, 3533–3539.
31 U. Mayer, V. Gutmann and W. Gerger, *Monatsh. Chem.*, 1975, **106**, 1235–1257.
32 Y. Marcus, *J. Solution Chem.*, 1984, **13**, 599–624.
33 J. Alarcon-Esposito, R. Contreras, R. A. Tapia and P. R. Campodonico, *Chem.–Eur. J.*, 2016, **22**, 13347–13351.
34 V. Gutmann, *Electrochim. Acta*, 1976, **21**, 661–670.
35 H. Inoue, Y. M. Liang, T. P. Yamada and O. B. O. Kimizuka, *Chem. Commun.*, 2020, **56**, 7013–7016.
36 A. J. Debethune, T. S. Licht and N. Swendeman, *Chem. Ind.*, 1958, 1364–1365.
37 C. M. Flynn, *Chem. Rev.*, 1984, **84**, 31–41.
38 C. S. Babu and C. Lim, *J. Phys. Chem. B*, 1999, **103**, 7958–7968.
39 W. Brostow, *Chem. Phys. Lett.*, 1977, **49**, 285–288.
40 C. L. Kneifel, M. D. Newton and H. L. Friedman, *J. Mol. Liq.*, 1994, **60**, 107–145.



 